An efficient finite element simulation method for additive manufacturing process

Qingyi Liu[1], Chaoyang Wang[1], Peng Yan[1*], Hui Ruan[1], Haozhou Xue[1], Leiting Dong[1*]
[1]School of Aeronautic Science and Engineering, Beihang University, Beijing, 100191, China

Abstract Accurate and efficient simulation of the thermal stress that occurs during the wire and arc additive manufacturing process plays an important role in the optimization of additive manufacturing processes. To improve the accuracy of the numerical simulations, we propose a two-stage modeling method in this work to reduce the number of artificial parameters required to perform the simulation. In the first stage, the single pass deposition process is simulated to calibrate the heat source parameters. Then, during the second stage, the component additive process is simulated using these calibrated parameters. To verify the proposed modeling method, wire and arc additive manufacturing experiments to fabricate a small step-shaped component and a large wall-shaped structure are performed. Comparison of the results obtained for the temperature field and the residual stress shows that the numerical results obtained using the two-stage modeling method show good agreement with the experimental results.

Keywords Wire and arc additive manufacturing; heat source calibration; numerical simulation; residual stress

1. Introduction

Additive manufacturing (AM) technologies offer the ability to produce near-net-shape components efficiently and accurately and AM has thus accumulated increasing attention in the manufacturing industry over the past 20 years because of the demand for increasingly high performance systems [1]. Wire and arc additive manufacturing (WAAM) combines arc welding technology with wire feeding technology and uses the arc as a heat source to manufacture metallic components layer-by-layer. Because of its low cost, high efficiency and capability for rapid near-net formation of large-sized complex components, WAAM has seen rapid development for application to fields including the automobile, shipbuilding and aerospace industries [2-4].

Components experience complex thermal cycles during the WAAM process and the large residual stresses produced during this process can lead to large-scale deformation and even cracking, which will seriously reduce the formation quality [6-8]. It is time-consuming to research the forming process and obtain an empirical summary if we rely on huge amount of experiments alone in additive manufacturing technology. Use of numerical simulation techniques such as finite element analysis allows the shortcomings of the experimental method to be overcome. Numerical simulation of the metal additive manufacturing process can predict the temperature field, the residual stress and the residual deformation effectively during the additive manufacturing process under specific process parameter conditions and the specimen quality can then be improved conveniently by optimizing the relevant process parameters, thus reducing manufacturing costs and shortening manufacturing times [9-12]. Ding studied a 3D thermo-elastic-plastic transient model and a model based on an advanced steady-state thermal analysis [13]. Huang developed simulation approaches that accelerated the additive manufacturing stress analysis process by considering the inherent thermomechanical features of direct energy deposition [11]. Although the geometry of the melt pool is critical during welding processes, the heat source parameters were not calibrated in these simulation techniques. Because of the difficulty involved in determining

*Corresponding authors. E-mail addresses: yanpeng117@buaa.edu.cn (P. Yan), ltdong@buaa.edu.cn (L. Dong).

these parameters accurately, the heat source parameters were usually recommended based on previous experience in welding simulation processes. The uncertainty in these input parameters will greatly reduce the accuracy and the reliability of the thermal and stress simulations performed for weld-based additive manufacturing. Additionally, in the conventional welding simulation field, where calibration of the input parameters has become common practice, the shape parameters of the weld pool (i.e., pool width and penetration) and the end crater geometry are commonly used to calibrate the heat source model. Azar calculated the heat source model based on experimentally observed weld pool sizes, and an analytical approach was used as an intermediate stage between the experiments and the numerical model [14]. Fu developed a neural network program to predict the parameters of Goldak's double-ellipsoidal heat source model [15]. Although these studies have contributed a great deal of research on heat source calibration for welding technology, some of the methods require complex analytical calculations and have not been applied directly to heat source verification for arc additive manufacturing to date.

Inspired by the heat source parameter calibration process used in welding simulations, a two-stage modeling method is proposed in this paper to reduce artificial setting of the parameters and obtain more accurate numerical simulation results for arc additive manufacturing. First, we introduce a theoretical model and a numerical simulation method for the additive process. Then, the single pass deposition process is simulated and the heat source parameters are calibrated by comparing the sizes of the molten pools obtained from the single pass deposition experiment. Finally, on the basis of the calibration of the heat source parameters, we simulate small-sized step components and large-sized wall structures; in addition, the temperature field and the stress field of the specimen during the printing process are then compared with the corresponding simulation results.

2. Theoretical formulation and numerical method

2.1 Theoretical Model

Arc additive manufacturing is a multi-factor coupling process that involves interaction of the welding wire, the arc and the matrix. This process has characteristics that include nonlinearity, non-steady-state operation, multi-pass processing, long process history and thermal coupling. In this paper, the thermal-mechanical sequential coupling method is used to simulate the temperature and stress behavior in the metal additive manufacturing process.

2.1.1 Thermal Analysis

The energy balance equation, i.e., the heat conduction equation, is expressed as [16]:

$$\rho C_P \frac{\mathrm{d}T}{\mathrm{d}t} = -\nabla \bullet \mathbf{q}(\mathbf{r}, t) + Q \tag{1}$$

where ρ is the material density, C_p is the specific heat capacity, T is the temperature, t is time, Q is the input heat, $\mathbf{r}$ is the relative position vector and $\mathbf{q}$ is the heat flux density according to Fourier's law of heat conduction, where

$$\mathbf{q} = -k\nabla T \tag{2}$$

where k is the thermal conductivity of the material.

The model temperature at the initial time is the ambient temperature, i.e.:

$$T(x, y, z, 0) = T_0 \tag{3}$$

where T_0 is the ambient temperature in the formula.

Heat is lost by both convection and radiation from the model surface. The convection-type heat dissipation is calculated based on Newton's law of cooling:

$$q_{con} = h(T - T_0) \tag{4}$$

where h is the convection coefficient. The value of h in this paper is 10 W/m^2/°C.

According to the Stefan-Boltzmann rule, the expression for radiative heat dissipation is

$$q_{rad} = \varepsilon\sigma(T^4 - T_0^4) \tag{5}$$

where ε is the radiation coefficient and σ is the Stefan-Boltzmann constant. In this paper, ε is equal to 0.54 [16].

2.1.2 Heat source model

In numerical simulation of the arc additive manufacturing process, the interaction between the arc and the metal material often deals equivalently with the heat source model [17]. In this paper, the Goldak double ellipsoid model is used as the heat source model in the numerical simulations [18]. This model is approximated by two semi-ellipsoids that have the same minor axis but different major axes, thus taking the actual geometry of the molten pool into account. A schematic diagram of the model is shown in Fig. 1.

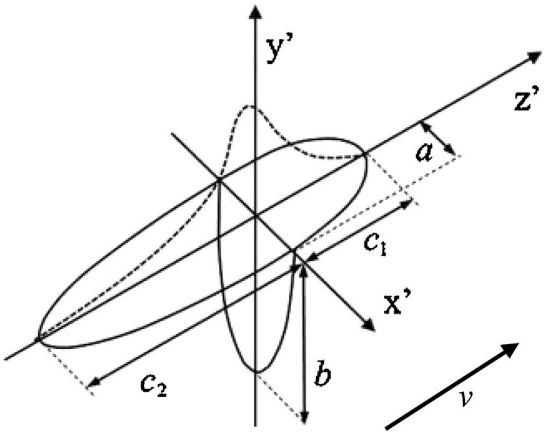

Fig. 1. Schematic diagram of Goldak double ellipsoidal model [19].

The heat source model is expressed as:

$$Q = \frac{6\sqrt{3}\eta P f_i}{\pi\sqrt{\pi}abc_i}\exp[-(\frac{3x'^2}{a^2} + \frac{3y'^2}{b^2} + \frac{3z'^2}{c_i^2})] \quad (i=1,2) \tag{6}$$

where P is the heat source power, η is the energy absorption rate, f_1 and f_2 are the energy distribution coefficients of the front and back ellipsoids, respectively, and must satisfy $f_1 + f_2 = 2$, and a, b, c_1 and c_2 are the heat source shape parameters.

2.1.3 Stress analysis

The temperature history of the model is obtained by performing a transient thermal analysis and the displacement field and the stress field of the model are then calculated via a quasi-static mechanical analysis. The stress balance equation is given as follows [10]:

$$\nabla \cdot \boldsymbol{\sigma} = 0 \tag{7}$$

From Eq. (7), the stress tensor $\boldsymbol{\sigma}$ is equal to:

$$\sigma = \boldsymbol{C}\boldsymbol{\varepsilon}_e \tag{8}$$

$$\boldsymbol{\varepsilon}_e = \boldsymbol{\varepsilon} - \boldsymbol{\varepsilon}_T - \boldsymbol{\varepsilon}_p \tag{9}$$

where $\boldsymbol{C}$ is the stiffness matrix, and $\boldsymbol{\varepsilon}$, $\boldsymbol{\varepsilon}_T$, $\boldsymbol{\varepsilon}_e$ and $\boldsymbol{\varepsilon}_p$ are the total strain, the temperature strain, the elastic strain and the plastic strain, respectively. The material model adopts the ideal elastic plastic model.

2.2 Simulation Strategy

2.2.1 Sequential thermal-mechanical coupling method

In this paper, the sequential thermal-mechanical coupling method is used to simulate both the temperature field and the stress field in the additive manufacturing process. The method is in two parts: first, a transient thermal analysis is performed to obtain the temperature field history of the component; second, the temperature field is applied as the initial load condition in the corresponding stress analysis model to calculate the displacement field and the stress field.

The additive process is realized via the birth and death element method. By modifying the stiffness of the element, entire model elements can be "killed" before the heat source is loaded. During the heat source loading process, the "killed" elements will be "activated" following the heat source.

2.2.2 Two-stage modelling method

To obtain more accurate numerical simulation results, we adopt the two-stage modeling method shown in Fig. 2. The first stage involves simulation of the single pass deposition process, and the heat source parameters are then calibrated via comparison of the sizes of the molten pools; on this basis, the second stage is simulation of the component additive process, from which the variations in the temperature field and the stress field with time will be obtained.

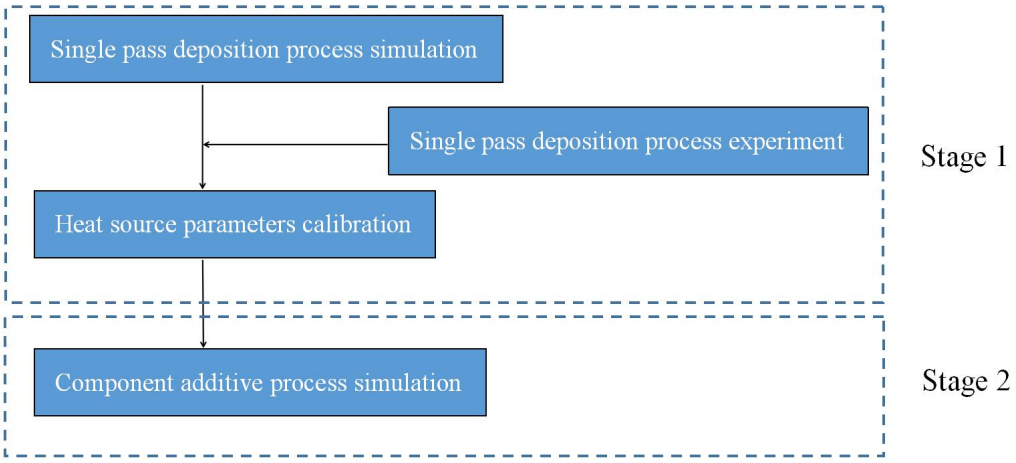

Fig. 2. Two-stage modeling method.

3. First stage – simulation of single pass deposition and calibration of heat source parameters

3.1 Single Pass Deposition Experiment

An arc fuse additive manufacturing system is used in the experiment and the parameters for the heat source parameter calibration experiment are shown in Table 1.

Table 1. Experimental process parameters for calibration of the heat source parameters.

Heat source power (KW)	Scan speed (m/min)	Wire feeding speed (m/min)	Wire diameter (mm)	Layer thickness (mm)	Dry elongation (mm)	Interlayer cooling (s)
4	0.5	6.5	1.2	1.5	15	30

To account for possible errors in printing, we printed three welds on a four-terminal fixed-supported substrate with a length of 150 mm, and the wire used is 316L stainless steel. An image of the welds is shown in Fig. 3.

Fig. 3. Three weld beads for use in the heat source parameter calibration experiment.

Each welding pass is cut into three samples along the cross-section of each welding pass stability section and one sample is cut longitudinally along the central line of the weld on extinguishing of the arc. Macroscopic metallographic samples of the weld are shown in Fig. 4.

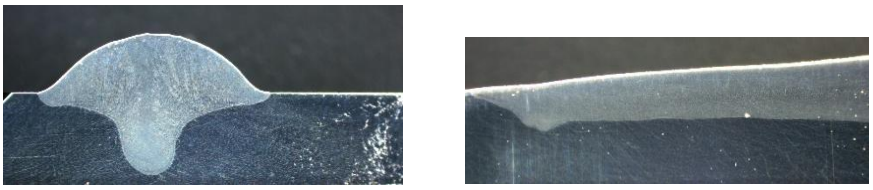

(a) Cross-section specimen. **(b) Longitudinal specimen.**

Fig. 4. Macro metallography images of the specimens.

The weld shapes and sizes are recorded under the microscope, the results for the shape parameters are taken as the average value for each group, and the process parameters for the molten pool are as shown in Table 2:

Table 2. Shape parameters for the molten pool.

Parameters	Deep penetration d	Melting width w	Length l
Size (mm)	3.157	9.515	16.431

Assuming that the heat source shape parameter is proportional to the shape parameter of the molten pool and that the proportional coefficient is α, the shape parameter expressions for the heat source are:

$$a = \alpha w/2\ ,\ b = \alpha d\ ,\ c_1 = a\ ,\ c_2 = \alpha l \tag{10}$$

The following equation is derived from Eq. (6) with these shape parameter expressions:

$$Q_1 = \frac{24\sqrt{3}Pf_1}{\pi\sqrt{\pi}w^2 d}\frac{\eta}{\alpha^3}\exp\left[-\frac{1}{\alpha^2}\left(\frac{12x'^2}{w^2}+\frac{3y'^2}{d^2}+\frac{12z'^2}{w^2}\right)\right]$$
$$Q_2 = \frac{12\sqrt{3}Pf_2}{\pi\sqrt{\pi}wdl}\frac{\eta}{\alpha^3}\exp\left[-\frac{1}{\alpha^2}\left(\frac{12x'^2}{w^2}+\frac{3y'^2}{d^2}+\frac{3z'^2}{l^2}\right)\right] \quad (11)$$

It is obvious that the heat source model expression can be simplified as a function of both the proportional coefficient α and the energy absorption rate η. The energy absorption rate is related to the welding method, the welding process parameters and the types of welding materials used. The argon arc welding heat source energy absorption rate of the equipment used in this work is generally 0.7–0.8. The calibration can be completed by combining the results of the experiments and the numerical simulation methods.

3.2 Numerical Simulation of Single Pass Deposition Process

A model of the heat source parameter calibration experiment is established as shown in Fig. 5. The dimensions of the weld bead are 150 mm×10 mm×1.5 mm.

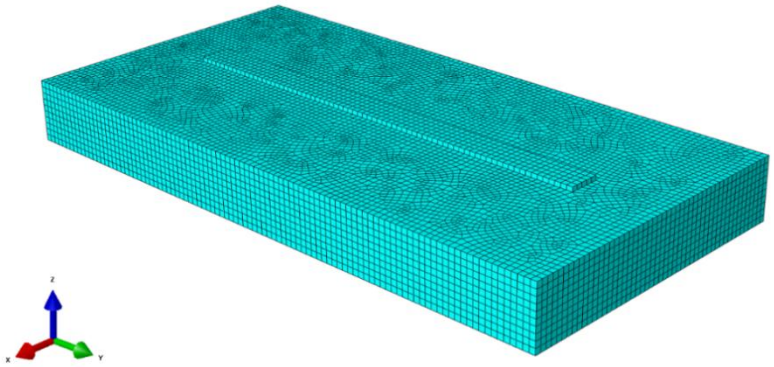

Fig. 5. Finite element model of the heat source parameter calibration experiment.

By adjusting the proportional coefficient α and the energy absorption rate η in Eq. (11) for the heat source model while also ensuring that the other process parameters remain the same as those in the experiment, the temperature field simulation is performed. When the width and depth of the molten pool in the simulation are consistent with their experimental values (Fig. 6), the proportional coefficient α and the energy absorption rate η can be determined.

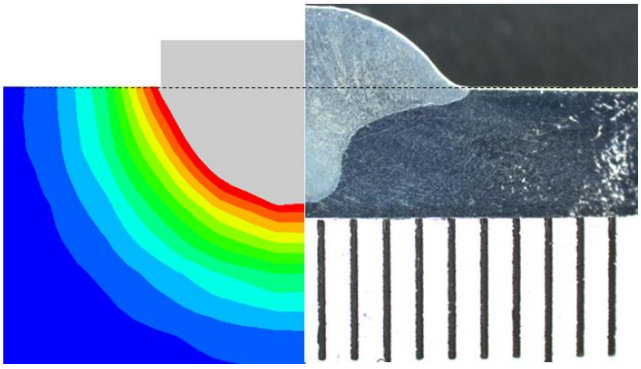

Fig. 6. Comparison of the width and depth of the molten pool obtained via simulations and experiments.

3.3 Calibration of Heat Source Parameters

When the energy absorption rate is 0.75 and the proportionality coefficient α is 0.9375, the

width and depth of the molten pool in the numerical simulation are highly consistent with the values in the experiment, and the heat source shape parameters are then obtained as shown in Table 3:

Table 3. Heat source shape parameters.

Parameters	*a*	*b*	c_1	c_2
Size (mm)	4.46	2.96	4.46	15.404

4. Second stage – numerical simulation and experimental verification of the component additive manufacturing process

4.1 Additive Experiment for Step-Shaped Component

Based on the calibration of the heat source parameters performed in the previous section, the temperature in the manufacturing process of a step-shaped component is studied in this section.

In the experiment, the substrate is fixed on four sides, the dimensions of the substrate are 400×400×20 mm, the height of each step is 24 mm, the wall thickness is 10 mm, and the lengths of the steps are 120 mm, 180 mm and 240 mm. As a result of collisions between the gun and the torch during the experiment, there was an interruption of 11 minutes when printing to the 4th layer; the corresponding interruption when printing to the 16th layer was 4 minutes. After the printing process is completed, the components and the substrate were cooled naturally to near room temperature. The printed step component and the substrate are shown in Fig. 7.

Fig. 7. Step component after printing.

The positions of the temperature measurement points used in the experiment are shown in Fig. 8.

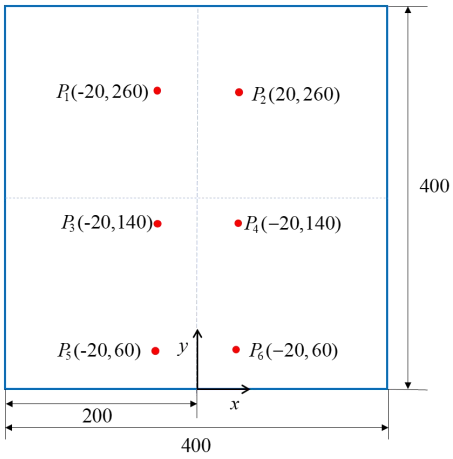

Fig. 8. Temperature measurement points for the step component.

The temperature curves for each temperature measurement point that was measured in the experiment are shown in Fig. 9. The sudden temperature drops shown in the picture at the beginning of printing and during printing resulted from the interruptions to the experiment caused by the torch hitting the gun, as mentioned above.

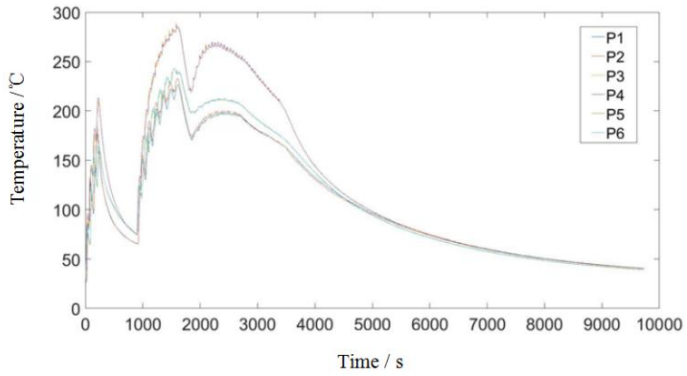

Fig. 9. Experimental temperature curves for each measurement point.

4.2 Additive Simulation of Step Component

The size of the finite element model of the step component remains the same as that in the experiment and has a total of three steps, as shown in Fig. 10.

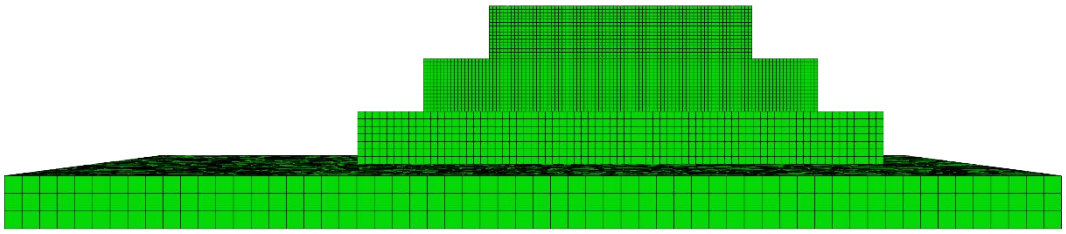

Fig. 10. Finite element model of the step component.

The numerical and experimental temperature results for the temperature measurement points selected on the upper surface of the substrate are shown in Fig. 11. Though the convection coefficient, emissivity, and thermal conductivity are all from the literature that have not been calibrated, which will cause some errors, the experimental and simulated results still show good agreement.

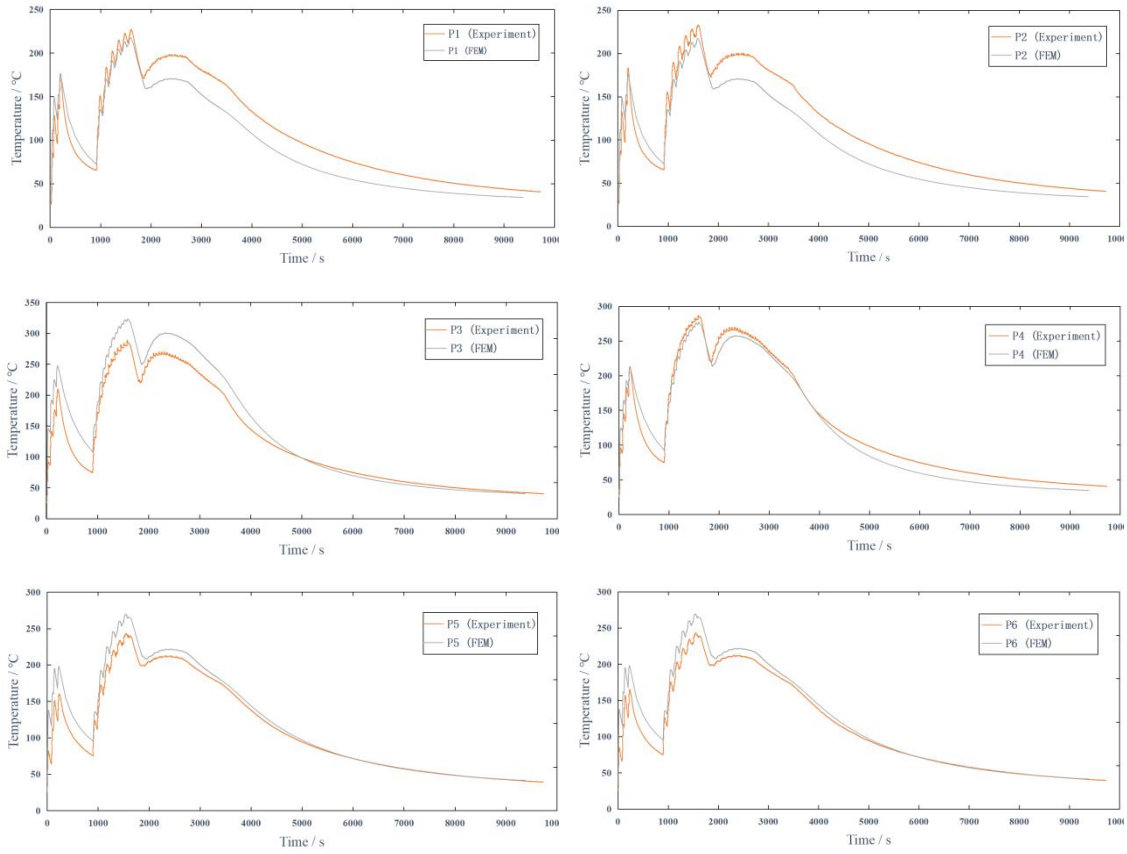

Fig. 11. Temperature curves recorded at each measurement point.

4.3 Additive Experiment for Wall Structure

To ease measurement of the substrate deformation in the experiment, one section of the substrate is fixed and the other section is freestanding, and the dimensions of the substrate are 800 mm×400 mm×20 mm. When printing is complete, the components and the substrates are cooled naturally to nearly room temperature, and the specimens and substrates are as shown in Fig. 12.

Fig. 12. Wall structure after printing.

The drilling method was used to measure the residual stress on the component surface and the position of reference points selected for the stress measurements are shown in Fig. 13.

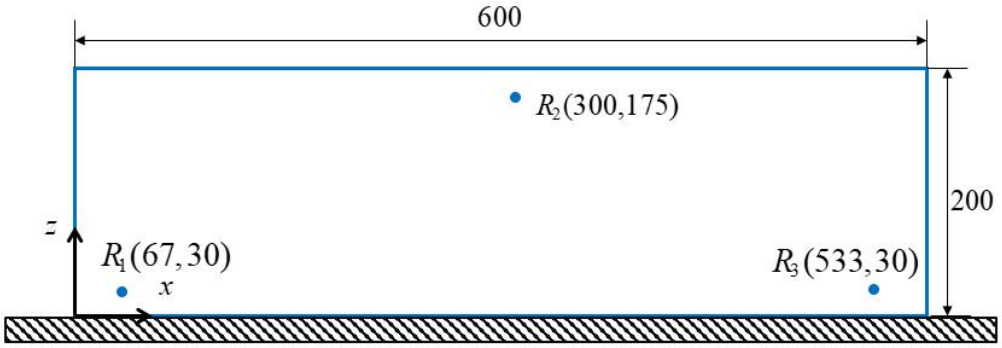

Fig. 13. Positions of the residual stress measurement points.

According to the GB/T 31310-2014 standard [19], we adopted type B rosette (BE120-2CA-K) comprising three single strain gage grids shown as Fig.14(a) to measure the relieved strains after the drilling step. The gage axes are oriented in each of three directions, (1) a reference direction, (2) 45° to the reference direction, and (3) perpendicular to the reference direction. The diameter and the depth of the drilled hole are both 2mm, and the diameter of the gage circle is 6mm and the calibration coefficients $\bar{a}$ and $\bar{b}$ are liner interpolated to be 11/75 and 3503/9000 respectively according to [19].

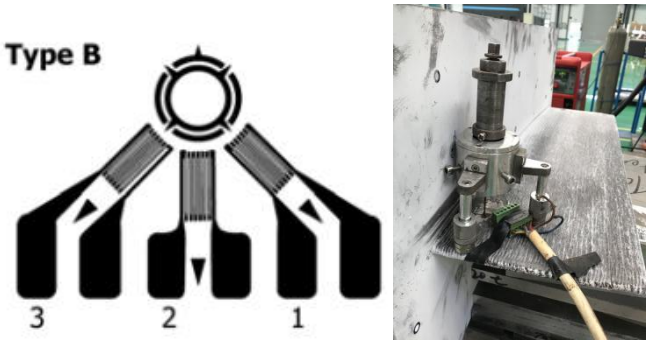

(a) (b)

Fig. 14. Positions of the residual stress measurement points.

The relieved strains of the three points measured in the experiment are listed in Table 4 below (x-axis defines as 0°, the counter-clockwise rotation defines as the positive direction).

Table 4. Experimental strain values (10^{-6}).

	0°	45°	90°
R_1	-212	-185	-37
R_2	-75	-84	-43
R_3	123	-22	-307

The residual stress values can be calculated at the selected residual stress measurement point on the component according to the equations(12) to (14) below:

$$p = \frac{\varepsilon_3 + \varepsilon_1}{2},\ q = \frac{\varepsilon_3 - \varepsilon_1}{2},\ t = \frac{\varepsilon_3 + \varepsilon_1 - 2\varepsilon_2}{2} \tag{12}$$

Where ε_1、ε_2、ε_3 represent the release strain in the three directions of 0°、45°、90° respectively. The three combination stresses P, Q and T can be computed corresponding to the three combination

strains p, q and t using:

$$P=\frac{\sigma_z+\sigma_x}{2}=-\frac{Ep}{\overline{a}(1+v)},\ Q=\frac{\sigma_z-\sigma_x}{2}=-\frac{Eq}{\overline{b}},\ T=\tau_{xz}=-\frac{Et}{\overline{b}} \tag{13}$$

$\overline{a}$、$\overline{b}$ are the calibration constants determined according to the hole diameter and type of rosette used, the in-plane Cartesian stresses σ_x、σ_z, and τ_{xz} can be derived:

$$\sigma_x=P-Q,\sigma_z=P+Q,\ \tau_{xz}=T \tag{14}$$

4.4 Additive Simulation of Wall Structure

The model is large in size and numerical simulation of the full scale model requires a great deal of time; it has also been verified that under the same simulating conditions, the results obtained for the full model and the half model are exactly the same. Therefore, a half model with dimensions of 600 mm×5 mm×200 mm is established for the numerical simulation, as shown in Fig. 15.

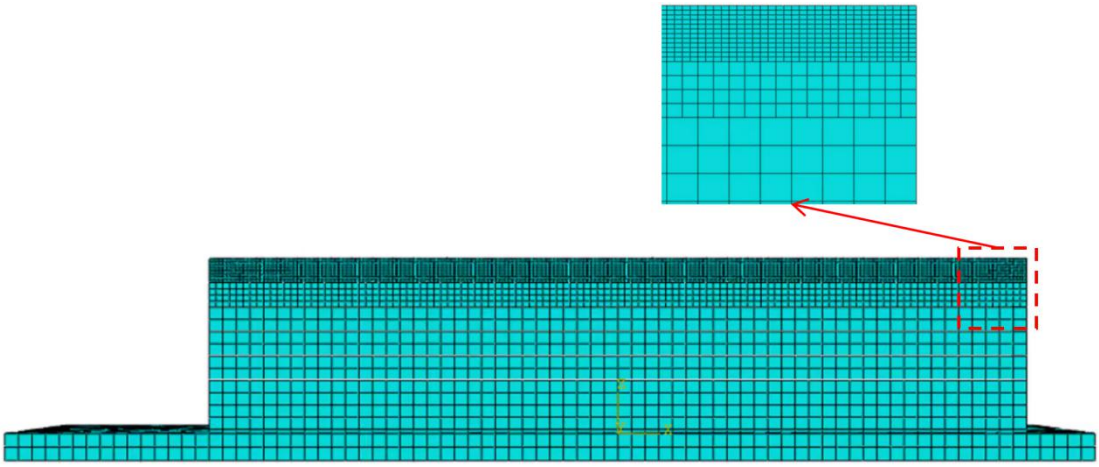

Fig. 15. Finite element model of wall structure.

The residual stresses at the measurement points of the wall structure are calculated using the drilling method as mentioned above. A comparison of the residual stresses from the numerical simulation with the corresponding experimental measurement results at the selected residual stress measurement points R_1, R_2 and R_3 on the component is shown in Table 5.

Table 5. Comparison of simulated and experimental stress results.

Vertical residual stress value σ_z （MPa）	Experimental results	Simulation results
R_1	180.7	203.8
R_2	72.1	93.5
R_3	212.9	221.7

The results in the table show that the errors in the stress results from the numerical simulation and the experimental measurements at the three points are greatly consistent, which indicates that the numerical simulation method can predict the stress accurately.

5. Conclusion

This paper proposes a two-stage modeling method to simulate the thermal stress in the arc additive manufacturing process. In the first stage, a numerical simulation of the single pass deposition process is performed and the heat source parameters are calibrated by comparison with the shape of the molten pool measured during the single pass additive manufacturing experiment. In the second stage, using calibrated heat source parameters, the additive manufacturing process for components is simulated and the temperature and stress fields are calculated. The method reduces the number of parameters to be set artificially. We then printed small-sized step-shaped components and a large-sized wall-shaped component. By comparing the numerical simulation results and the experimental temperature and stress results at the reference points in the additive manufacturing process, it can be concluded that for the step components and the wall structure, the results of the experiments are in good agreement with the simulation results, thus verifying the validity of the method proposed in this paper.

Acknowledgments

Funding: This work was supported by the National Defense Special Zone for Science and Technology Innovation of China, the Aviation Science Foundation of China and the Fundamental Research Funds for the Central Universities. We thank David MacDonald, MSc, from Liwen Bianji, Edanz Editing China (www.liwenbianji.cn/ac), for editing the English text of a draft of this manuscript.

References

[1]K.E.K.Vimal, M.N. Srinivas, S. Rajak, Wire arc additive manufacturing of aluminium alloys: A review, Materials Today: Proceedings.(2020).

[2]C.J. Smith, S. Tammas-Williams, P.S. Mahoney, et al. 3D printing a jet engine: An under-graduate project to exploit additive manufacturing now and in the future[J]. Materials Today Communications, 2018, 16: 22-25.

[3]C.R. Cunningham, J.M. Flynn, A. Shokrani, Invited review article: Strategies and processes for high quality wire arc additive manufacturing, Additive Manufacturing. 22 (2018) 672-686.

[4]T.A.Rodrigues, V. Duarte, R.M. Miranda, Current Status and Perspectives on Wire and Arc Additive Manufacturing (WAAM), Materials. 12(7) (2019) 1121.

[5]F. Hajializadeh, A. Ince, Finite element–based numerical modeling framework for additive manufactur-ing process, Material Design & Processing Communications. 1(1) (2019) 28.

[6]E.R. Denlinger, J.C. Heigel, P. Michaleris, Residual stress and distortion modeling of electron beam direct manufacturing Ti-6Al-4V, Proceedings of the Institution of Mechanical Engineers, Part B: Journal of Engineering Manufacture. 229(10) (2015) 1803-1813.

[7]T. Mukherjee, W. Zhang, T. DebRoy, An improved prediction of residual stresses and distortion in additive manufacturing, Computational Materials Science. 126 (2017) 360-372.

[8]R. Li, J. Xiong, Y. Lei, Investigation on thermal stress evolution induced by wire and arc additive manufacturing for circular thin-walled parts, Journal of Manufacturing Processes. 40 (2019) 59-67.

[9]P. Nandwana, A. Plotkowski, R. Kannan, S. Yoder, et al. Predicting geometric influences in metal additive manufacturing[J]. Materials Today Communications, 2020, 25: 101174.

[10]E. Denlinger, J. Irwin, P. Michaleris, Thermomechanical modeling of additive manufacturing large parts, Journal of Manufacturing Science and Engineering. 136(6) (2014) 061007.
[11]H. Huang, N. Ma, J. Chen, Toward large-scale simulation of residual stress and distortion in wire and arc additive manufacturing, Additive Manufacturing. (2020) 101248.
[12]S. Jayanath, A. Achuthan, A computationally efficient finite element framework to simulate additive manufacturing processes, Journal of Manufacturing Science and Engineering. 140(4) (2018).
[13]J. Ding, P. Colegrove, J. Mehnen, Thermo-mechanical analysis of Wire and Arc Additive Layer Manufacturing process on large multi-layer parts, Computational Materials Science. 50(12) (2011) 3315-3322.
[14]A.S. Azar, S.K. Ås, O.M. Akselsen, Determination of welding heat source parameters from actual bead shape, Computational materials science. 54 (2012) 176-182.
[15]G. Fu, J. Gu, M.I. Lourenco, Parameter determination of double-ellipsoidal heat source model and its application in the multi-pass welding process, Ships and Offshore Structures. 10(2) (2015) 204-217.
[16]J.C. Heigel, P. Michaleris, E.W. Reutzel, Thermo-mechanical model development and validation of directed energy deposition additive manufacturing of Ti-6Al-4V, Additive manufacturing. 5 (2015) 9-19.
[17]C. Li, E.R. Denlinger, M.F. Gouge, Numerical verification of an Octree mesh coarsening strategy for simulating additive manufacturing processes, Additive Manufacturing. 30 (2019) 100903.
[18]J. Goldak, A. Chakravarti, M. Bibby, A new finite element model for welding heat sources[J]. Metallurgical transactions B, 1984, 15(2): 299-305.
[19]Metallic material-determination of residual stress-Hole drilling strain-gauge method. Beijing: Standards Press of China. 2014.